Simultaneous multi-filter photometric characterization of space debris at the Swiss Optical Ground Station and Geodynamics Observatory Zimmerwald

Emiliano Cordelli
Astronomical Institute University of Bern, Sidlerstrasse 5, CH-3012 Bern, Switzerland
Peter Schlatter
Astronomical Institute University of Bern, Sidlerstrasse 5, CH-3012 Bern, Switzerland
Thomas Schildknecht
Astronomical Institute University of Bern, Sidlerstrasse 5, CH-3012 Bern, Switzerland

ABSTRACT

The Astronomical Institute of the University of Bern (AIUB) is performing space debris research for the past 25 years. The main research topics include the search for and the discovery of space debris objects, the build-up and maintenance of a catalogue of space debris orbits, and the physical characterization of debris objects by fusing astrometric, photometric and spectroscopic data. In particular, all these tasks are performed using data from the AIUB telescopes at the Swiss Optical Ground Station and Geodynamics Observatory Zimmerwald.
We will present the results of a space debris characterization campaign performed with the newly installed multipurpose twin sensor consisting of two 40 cm wide-field telescopes. The configuration of this sensor allows using it for three main purposes: the discovery of faint objects due to its aperture and its wide field of view, the follow-up and recovery of cataloged objects, and their characterization as each telescope is equipped with a color filter set. The latter allows for simultaneous observations in two color bands, a prerequisite to derive color indices of rotating or tumbling objects. In this paper, we will present the results of a campaign performed to characterize functional satellites and debris in GEO and MEO regions. Particular attention will be given to defunct GLONASS satellites. This study provides important information regarding the rotational state, the shape, and the surface material of objects. This information may be used to recognize objects when building up and maintaining catalogs, as well as may facilitate the identification of a candidate parent's object of fragments. This analysis is performed exploiting the photometric data acquired with sensors of the Zimmerwald observatory.

1. INTRODUCTION

The space race, started in 1957 with the launch of Sputnik 1, had also a new side product: space debris. The space debris constitutes a serious danger for actual and future operational satellites and manned space flight. Furthermore, prediction says that the number of space debris is increasing leading to an increment of the collision among space objects [1].
It is a common agreement that to preserve the future usage of the outer space the application of mitigation measures is mandatory. At the moment, the mostly used mitigation methods are constituted by a forced disposal in the atmosphere or the disposal into a graveyard orbit after the end of the satellite life [2]. Nevertheless, to stabilize the growth of space debris the so called Active Debris Removal (ADR) mission may also be necessary [3].
Fundamental for the ADR missions is the accurate knowledge of the object position, of its attitude state, and of its evolution over time. This kind of information can be retrieved via different techniques as optical observations [4], satellite laser ranging [5] and radar imaging [6]. In particular, by analyzing the light curves, the variation over time of the amount of light reflected by the object, one can determine the spin period [4, 7], the spin axis direction [8], and as in the classical astronomy also the shape of the object [9].
The analysis of the colors and of the color indices of the light reflected by the studied object provides further information about its physical and attitude properties. In particular, by comparing laboratory [10] and real satellite measurements one could infer the material, the age, and therefore the possible parents of debris object [11, 12, 13].
In this paper we will show the results obtained by a preliminary study to investigate the benefits given by the analysis of the colors and of the color indices on the attitude determination. This is possible thanks to the synchronous observations in different color bands with two telescopes. The main advantage of this technique is given by the fact that we can analyze the contribution, given by the object, or a portion of it, under exactly the same condition.

The study will focus on both active and defunct satellites, and on rocket stages in different orbital regimes. First, a brief description of the used telescope and of the procedure to acquire and extract data is given; second, the results for GEO three-axis stabilized satellites, for different spent rocket bodies, and of spent Glonass satellites are reported. Finally, the advantages and the weak points of the proposed technique are analyzed.

2. TELESCOPE CHARACTERISTICS

All the observations were performed from the newly implemented Zimmerwald Twin Widefield Instrument (ZimTWIN) telescope located at the Swiss Optical Ground Station and Geodynamics Observatory Zimmerwald (46.8772 N, 7.4652 E, 951.2 m). As can be seen from Fig. 1 and Table 1, the telescope consists of two 40 cm tubes with f/2.4 primary focus. Both tubes are equipped with the same hardware in terms of controllers and CCD cameras. This choice was made on purpose to obtain the same performances, in terms of sensitivity and exposure characteristics, for each tube.
The camera covers a field of view (FoV) of 2.14 x 2.14 degrees per tube making the telescope also suitable for survey applications. Each tube is equipped with a filter unit, and by aligning the pointing direction of the tubes it is possible to perform synchronous multi-filter photometry.
The readout time for a full frame is about 8 seconds, nevertheless the camera allows the selection of a subframe which shortens the readout time to 1.5 seconds (for the subframe dimensions used for this study) allowing us to increase the sampling frequency.
The telescope is equipped with a high-transmission BVR set of filters, which transmissivity curves are shown in Fig. 2. To have simultaneous observations in the different colors we needed to split the set and we put B and R in tube 1, and V in tube 2, respectively.
Finally, the mount is an equatorial mount whose tracking speed is up to 13 degrees/seconds which doesn't limit us in the object choice; however we focused on MEO and GEO objects to find the best compromise between the rotation period of the object, the sampling frequency, and the time needed to obtain a good set of measurements.

Fig. 1 The ZimTWIN Telescope.

Table 1 Summary of the characteristics of the ZimTWIN telescope.

	Tube 1	**Tube 2**
Tube	ASA 16 inch Deltagraph f/2.4	ASA 16 inch Deltagraph f/2.4
Aperture	40 cm	40 cm
Focal Length	96 cm	96 cm
Camera	FLI PL16803 – Front illuminated	FLI PL16803 – Front illuminated
Sensor	36.9 x 36.9 cm, 4096 x 4096 pixels	36.9 x 36.9 cm, 4096 x 4096 pixels
Pixel size	9 μm	9 μm

Field of View	2.14 x 2.14 degree	2.14 x 2.14 degree
Pixel scale	1.88 arcsec/pixel	1.88 arcsec/pixel
Filter	B and R	V
Mount	ASA DDM160-Absolute TWIN	

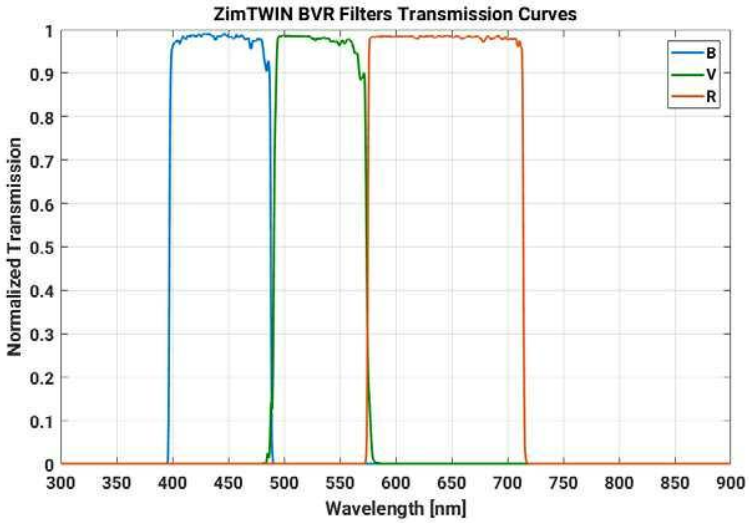

Fig. 2 Filters Transmission Curves.

3. MEASUREMENTS ACQUISITION AND PROCESSING

To carry out this experiment we controlled the two cameras and the mount independently using the software provided with the telescope. Therefore, we steered the mount to track the object, using TLE, and started the two cameras manually. This avoided delays or huge desynchronization between the cameras due to the interaction of the tube 1 with the mount. At the same time, the manual start limits the perfect synchronization of the cameras.

The object tracking allowed us to set up for each camera a relatively small region of interest (ROI) around the object. This helped reducing the camera readout time from ca. 8 (of the full frame) to 1.5 seconds, and increase the sampling frequency to one image every 6.5 seconds (with an exposure time of 5 seconds). All the following measurements were acquired with a square ROI of 250 pixels side; only for the ASTRA1 case a square ROI of 400 pixels was used (the ROI contains all 4 ASTRA1 satellites as shown in Fig. 4).

The use of the ROI allowed us to acquire long light curves with a high sampling rate (up to more than 70 minutes for ASTRA1 with 800 measurement points, see Section 4.1). The ROI allowed us also to optimize the signal to noise ratio (S/N) via using short exposure times, and reducing the amount of thermal noise and of signal coming from the sky background (as happen if we sidereal track a star field and let the object cross it). On the other hand, this technique, due to the small dimensions of the ROI, obliged us to acquire additional Landolt star-fields for the magnitude calibration [14].

To overcome the problem of the not perfect time alignment of the images acquired by the two tubes, we synchronized the clocks of the controllers, of the mount and of the CCD cameras, to the same ntp-server. We could in this way monitor the eventual drift in the images acquisition and correct it in processing.

The processing of the measurements can be divided into two main steps: the raw images analysis, and the light curve and color index creation and processing.

The first part is performed using an open source software: AstroImageJ [15], within the software is possible to perform both the raw image calibration applying bias, dark, flat field images, and to analyze the flux of the target objects. This software was used first to extract the magnitude zero-point coming from the reference Landolt stars; second to extract from the single pictures all the information needed for light curve processing. The images are processed using the aperture photometry method: three concentric circles with different radius are set up, depending on the brightness of the object, to extract the flux given by the object and the sky background. For the light curve processing we essentially

used the background subtracted flux associated with the object (later called source-sky), the exposure time, the reference epoch of the measurements (start of exposure), and the error of the flux associated with the object. After the extraction of the data, a visual inspection is carried out to reject those images where the area of the object was contaminated by a star streak.
The second part of the processing is performed in Matlab. In a first step, the net fluxes are converted to magnitudes according to Eq. (1).

$$M_i = -2.5\, log_{10} \frac{F_i}{t} + K_i \tag{1}$$

Where:

- M_i is the magnitude with the ith filter (respectively B, V, and R),
- F_i is the measured flux of the objects without the sky contribution of the ith filter,
- t is the exposure time,
- K_i is the magnitude zero-point for the ith filter which was determined using the Landolt stars.

The error associated to the measured light curves and to the color index, visible later in the results, is derived from the error associated to the flux of the object by applying the standard error propagation law.

$$\sigma_M = \frac{\partial M}{\partial F} \sigma_F = -2.5 \frac{1}{F} \frac{1}{ln\, 10} \sigma_F \tag{2}$$

$$\sigma_{CI} = \sqrt{\sigma^2_{M_{B/R}} + \sigma^2_{M_V}} \tag{3}$$

Where:

- σ_M, σ_{M_i} are the magnitude error and the magnitude error w.r.t. the ith filter (respectively B, V, and R),
- σ_F is the error associated to the source-sky flux,
- σ_{CI} is the color index error.

The time difference between the images acquired from the two tubes is also monitored. Although the hardware and the way of operating is identical for both tubes, sometimes we experienced a drift in the start of exposure epochs which reached 3 seconds after 70 minutes of continuous acquisition of images. The cause of it is still under investigation. Even if the effects of the time drift, considering the attitude motion of the observed target, are negligible we wanted to correct them exploiting the synchronization of the mount and camera controllers to the same ntp-server. We interpolated the flux measurements with a smoothing spline in order to preserve the shape of the light curve and to extract the flux values at precise time epochs common to both tubes. This because we are interested in the contribution given by the same parts of the satellite, under the same illumination conditions, in the color of the reflected light. The interpolated flux is then compared with the measured one to fine tune the amount of smoothing provided by the spline. The tuning of the spline was done independently for each study case. The interpolated flux is also used to calculate the color index which is then compared with that obtained from the measurements. As we will see in the following sections, this method allowed us to correct for the time drift and to obtain smoothed color indices which are easier to interpret.

4. OBSERVATION RESULTS

To optimize the S/N ratio for each filter and for each object we used exposure times between 3 and 5 seconds, with a consequent sampling interval between 4.5 and 6.5 seconds. The achieved sampling rate constitutes a limit in the choice of the observed objects; we have chosen targets whose rotation period is longer than 2 minutes in order to avoid undersampling of light curves and respective color indices. Since the attitude information we are looking for are in the periodical changes of the color index, taking into account the limitations given by the telescope system, and by the sampling rate we conducted this first study on objects with long visibility windows; we then focus on MEO and GEO objects.

In the following sections we will analyze the results obtained from stable satellites, from relatively simple shaped objects (the rocket bodies could be considered in first approximation as cylinders), and from more complex shaped satellites (as Glonass) in a tumbling motion.
To better understand the obtained results we show in Fig. 3 some pictures of the observed objects.

Fig. 3-a ASTRA 1KR [16]

Fig. 3-b ASTRA 1N [16]

Fig. 3-c DELTA 4 R/B Medium [17]

Fig. 3-d ATLAS 5 R/B - CENTAUR Upper stage [18]

Fig. 3-e GLONASS (Uragan) [16]

Fig. 3-f GLONASS M (Uragan-M) [16]

Fig. 3 Representation of the observed objects.

4.1 THE ASTRA1 CLUSTER

To obtain an understanding of the achievable results we focus first on three-axis stabilized satellites. In particular, we performed several observations of the ASTRA1 cluster. This is constituted of 4 GEO satellites all active and controlled very close together. In fact, as we can see from Fig. 4, these are within a square ROI of 400 pixels side, equivalent to a region of 12.5 x 12.5 arcmin. The usage of a ROI of 400 pixels allowed us to carry out one single series of exposures and extract the light curves and the respective color indices for 4 different satellites under the same sky and illumination conditions.

The ASTRA1 cluster is constituted respectively of the ASTRA1KR, ASTRA1L, ASTRA1M, and ASTRA1N satellites (whose respective COSPAR ID are 06012A, 07016A, 08057A, and 11041A). Since the aim of this study is not the identification of the objects we just called them "Sat1", "Sat2", "Sat3", and "Sat4" as shown in Fig. 4. An extract of the results obtained for this cluster with the V and R filters can be seen in Fig. 5 and Fig. 6, respectively for "Sat2" and "Sat4". These figures summarize more than 70 minutes of measurements for a total of 800 images each one acquired with 4 seconds of exposure time.

This experiment was carried out since stabilized satellites should give at least in the short term a constant color index given by the fact that there are no huge changes in their attitude. Nevertheless, in the long term a change in the color index is expected because the solar panels are always pointing towards the Sun. Therefore the orbital motion, for increasing phase angle, will cause a decrease of the intensity of the light reflected by the solar panels toward the observer, allowing him to see the color of the bus of the satellite, or of a portion of it.

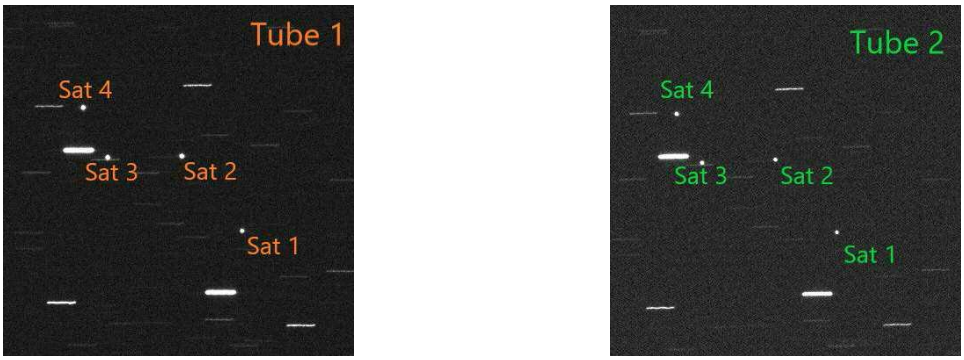

Fig. 4 ASTRA1 (KR, L, M and N satellites) Cluster from tube 1 with R filter (on the left) and from Tube 2 with V filter (on the right).

Although the illumination and environmental conditions were the same during the observation period for all satellites their light curves show 4 different behaviors. As one can see in Fig. 5 and Fig. 6, "Sat2" shows a general increase of the brightness with a temporary luminosity rise; while "Sat4" shows first a decrease with a successive increase of the brightness. It is interesting to notice how the light curves with the different filters show a similar trend dominated by the phase angle and the attitude of the satellite. On the other hand, the color indices, although pretty much constant over the observation period, show some important differences. From Fig. 5 one can see how in the presence of the temporary increase of the brightness, the color index is decreasing towards the blue/green colors which is probably due to a more "specular" reflection of a part of the satellite. Another aspect that is very important to notice is the value of the color indices, for "Sat2" is about 0.85 Mag while for "Sat4" is ca. 0.4 Mag. There are several possible reasons for these different values: the satellites have different busses, different ages and therefore different exposition times to the space environment, and finally different attitudes. These are in fact telecommunication satellites which provide services to European regions [19], therefore, the different busses and the pointing of their antennae will reflect differently the light towards the observer.

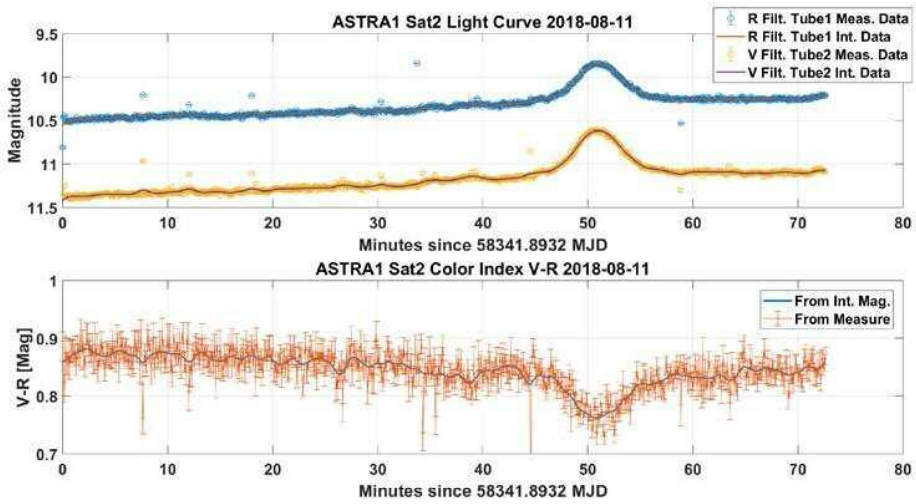

Fig. 5 Light curves with V and R filters extracted for ASTRA1 cluster "Sat2" (top) and color index (bottom).

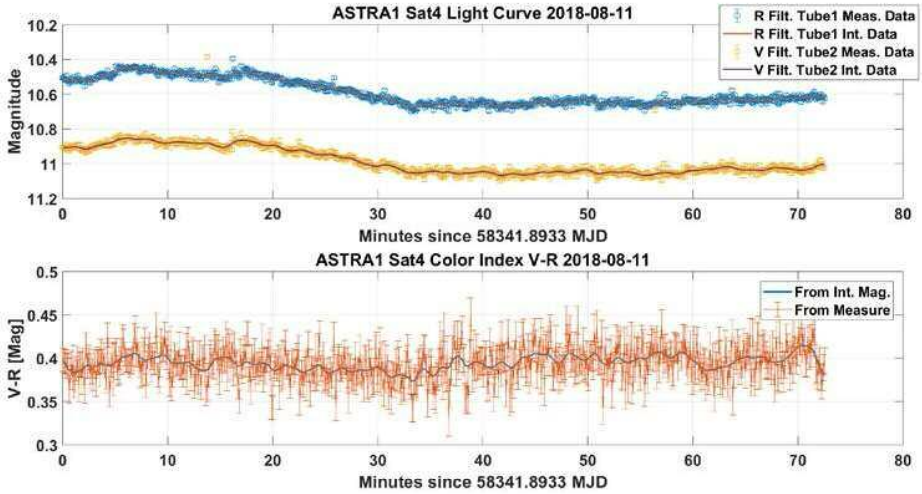

Fig. 6 Light curves with V and R filters extracted for ASTRA1 cluster "Sat4" (top) and color index (bottom).

4.2 THE UPPER STAGES

For the second study case we observed objects with a relatively simple shape in a tumbling motion. The upper stages (also called rocket bodies) can be considered, at least in a first approximation, as cylinders. This should produce relatively simple light curves which will be easier to interpret. We will report three examples constituted by two DELTA 4 R/B upper stages, and one ATLAS 5 - CENTAUR upper stage. These objects were chosen since their rotation period is higher than 400 seconds that allowed us to have more than 70 measurement points per period (assuming an exposure time of 4 seconds).

4.2.1 DELTA 4 R/B

We observed two DELTA 4 R/B, respectively the 11036B and the 15036B, belonging to different orbital regimes. The first, launched in 2011, since used for the disposal of a GPS satellite is placed in an almost circular “GPS-Graveyard” orbit; the second, launched in 2015, is placed into a high eccentric orbit (HEO), its semi-major axis is

39606 km and the eccentricity is 0.826. The first was observed with an exposure time of 4 seconds, the second, with 5 seconds. Both were observed with V and R filters within a square ROI of 250 pixels side.
Looking at the obtained results in Fig. 7 and Fig. 8, for 11036B and 15036B, respectively, we can notice the different behavior of the light curves. This may be due to a different observing geometry (orientation of the spin axis in the body-fixed and the inertial reference frame), or due to the fact that, although they are the same kind of upper stages, there are several versions used for different purposes which differ in their size. In particular, the first is the version Medium-plus 4,2 [20], and the second is the version Medium-plus 5,4 [21]. Furthermore the light curves in Fig. 7 show a more complex structure which could be due to the fact that the shape of the object, visible in Fig. 3-c, differs from a simple cylinder and that the rotation may occur around an intermediate axis and is not yet stable.
Looking at the respective color indices we can see how they show a clear periodicity coincident with the rotation period. The color indices show only one minimum per period while the light curves show two minima per period. Depending on the Sun-observer-object geometry, the primary and the secondary minima of the light curves in Fig. 8 could be comparable, while the signature of the color index is unambiguous. The signature of the color index could then provide indications about which end, either the top or the bottom, of the rocket body we are looking at. Finally, it is important to notice the difference in the average values of the color indices; for the first it is ca 0.6 Mag, for the second ca 0.7, which in our opinion is also a consequence of the different versions of the considered objects.

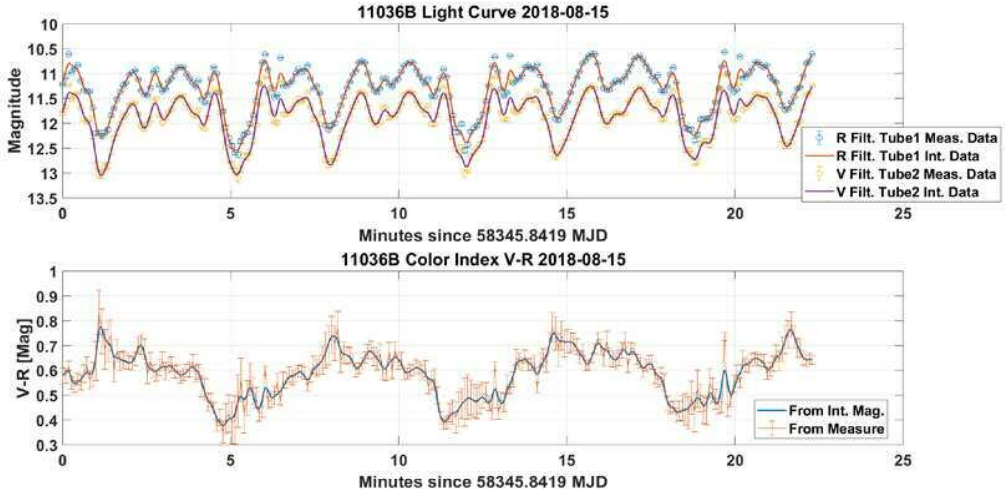

Fig. 7 Light curves with V and R filters extracted for the DELTA 4 R/B 11036B (top) and color index (bottom).

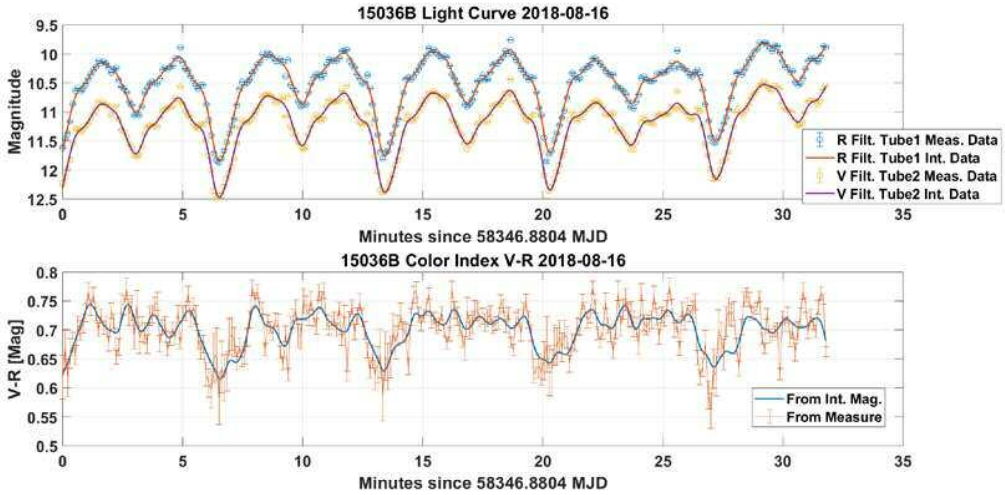

Fig. 8 Light curves with V and R filters extracted for the DELTA 4 R/B 15036B (top), and color index (bottom).

4.2.2 ATLAS 5 CENTAUR R/B

We observed a second upper stage in a "GPS-Graveyard" orbit. This is the case of an ATLAS 5 CENTAUR observed using a square ROI of 250 pixels side and 5 seconds of exposure time. This upper stage was observed first with the V and R filters, then a second series was acquired using the B and V filters. Comparing the light curves shown in Fig. 9 and Fig. 10 one can see that their behavior is more similar to what to expect from a cylinder shaped object: two maxima given by the side of the cylinder and two minima due to the top and bottom end of the "cylinder". Furthermore, the two minima are not as symmetrical as the two maxima, this is also expected due to the fact that on one end there is the mechanical interface to the payload, and on the other the nozzle of the propulsion system. It must be said that the light curves show also periodical brighter points caused by specular reflection of the object which are not taken into account from the smoothing spline. The specular reflection exclusion was done intentionally to have smoother color indices to better understand their general trend.
As in the previous case, the color indices show unambiguous periodical maxima, with higher uncertainty, which are coincident with the "absolute" minima of the light curves. Although the color indices show different noise levels (the B-V is noisier than the V-R due to the higher uncertainty of the B light curve which is the faintest), it is possible to see some common aspects. They both show periodical primary and secondary maxima, the secondary is occurring just after the secondary minima in the light curves. On the other hand, the color indices present some slightly different trends between the primary and secondary maxima. This last aspect probably indicates that the sides of the rocket are not identical.

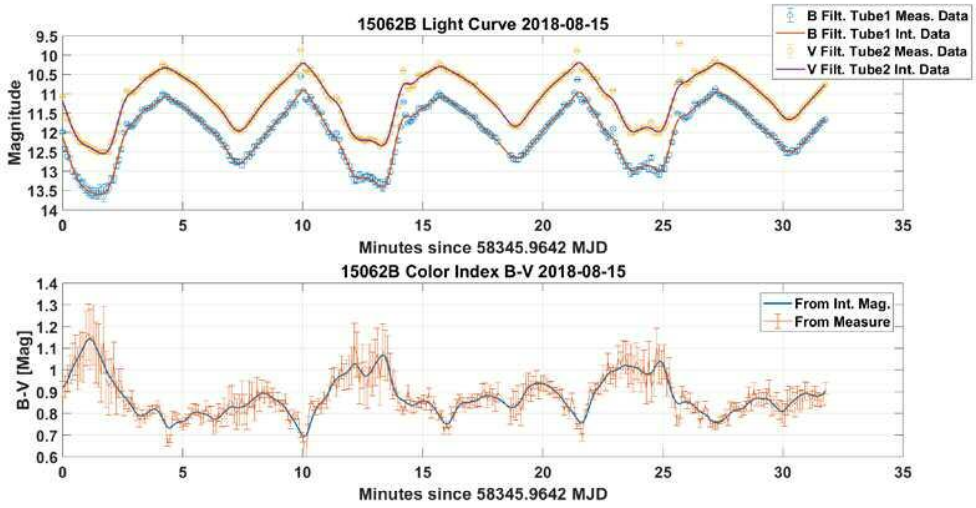

Fig. 9 Light curves with B and V filters extracted for ATLAS 5 CENTAUR R/B (top) and color index (bottom).

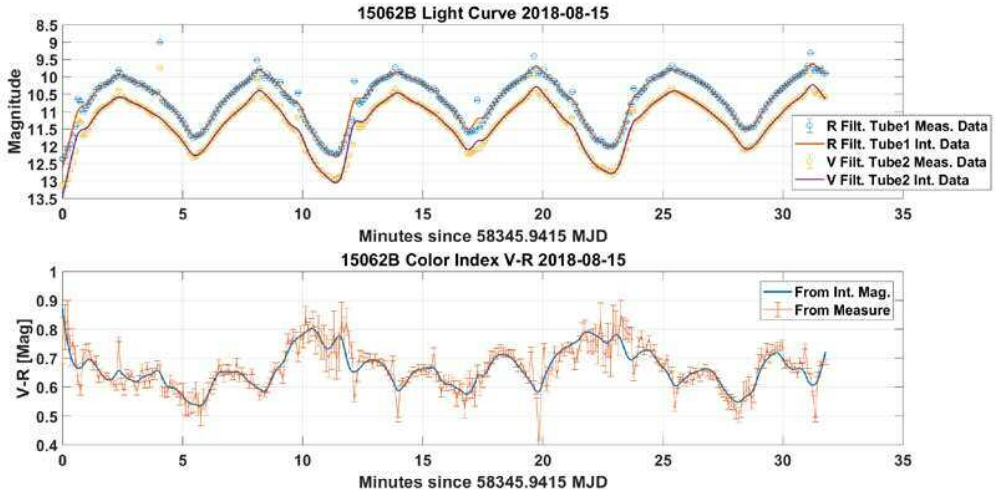

Fig. 10 Light curves with V and R filters extracted for ATLAS 5 CENTAUR R/B (top) and color index (bottom).

4.3 THE GLONASS SATELLITES

The last study case is constituted by objects in a tumbling motion with a more complex shape. We focused therefore on the decommissioned Glonass satellites. In the following section we will discuss the results obtained from 4 different Glonass satellites: two old ones launched in 1993 and 1995, respectively, and two belonging to the same launch in 2004 but with different bus type. The 93010C, 95037B, and the 04053A are examples of the old generation Glonass satellite called "Uragan" while the 04053B is a new generation Glonass-M satellite (Uragan-M) [16].
All following observations series were acquired using a square ROI of 250 pixels side, and an exposure time of 5 seconds.

4.3.1 93010C & 95037B

Fig. 11 and Fig. 12 show the light curves and the relative V-R color indices obtained for the two old generation Glonass satellites which are in space since more than 20 years. Both of them have a rotation period longer than 10 minutes. It is interesting to notice that, although the light curves show very similar structures, their color indices look completely different. The first has an average value of 0.85 Mag, and the second of ca 1 Mag. The latter shows a clear decreasing trend which could be caused by a change in the contribution of light reflected towards the observer either from the bus or the solar panel of the satellite. This contribution change is maybe caused by the decrease of the phase angle which would explain also the increase of the brightness shown in the light curves. To be precise also for the 93010C the phase angle is decreasing but its value, at the moment of the observation was ca 75 degrees while for the second less than 30 degrees.
Comparing now the two color indices it is interesting to notice the clear periodical signature visible for the 95037B case which is probably hidden by the noise for the 93010C. Looking at the bottom graph of Fig. 12 it is possible to see minima for the color index at minutes 10, 20, and 30 which coincide to the maxima visible in the light curves. I.e. these maxima in the light curve correspond to bluer surface areas compared to the areas corresponding the maxima in the light curve. Then it is also possible to see other sharper minima at the minutes 5, 15, and 25 also these coincident with the maxima at the same epoch in the light curves. Finally, it is interesting to notice the different behavior of the color index between the just mentioned maxima; in particular one should compare the trends from minutes 0 to 5, 10 to 15, and 20 to 25 with those from 5 to 10, 15 to 20, and 25 to 30. In the first series of trends a more monotonous increasing behavior is visible while for the second series another series of minima is visible (even if not so clearly from minutes 25 to 30). This signature clearly indicates that the one satellite side is different from the other, a feature that will be very useful for identifying the attitude. Nevertheless, it is difficult at this stage to identify which side of the satellite we are looking at, but this is a problem which could be solved by closer inspection of the surface materials based on open source data, or by laboratory measurements before the spacecraft launch.

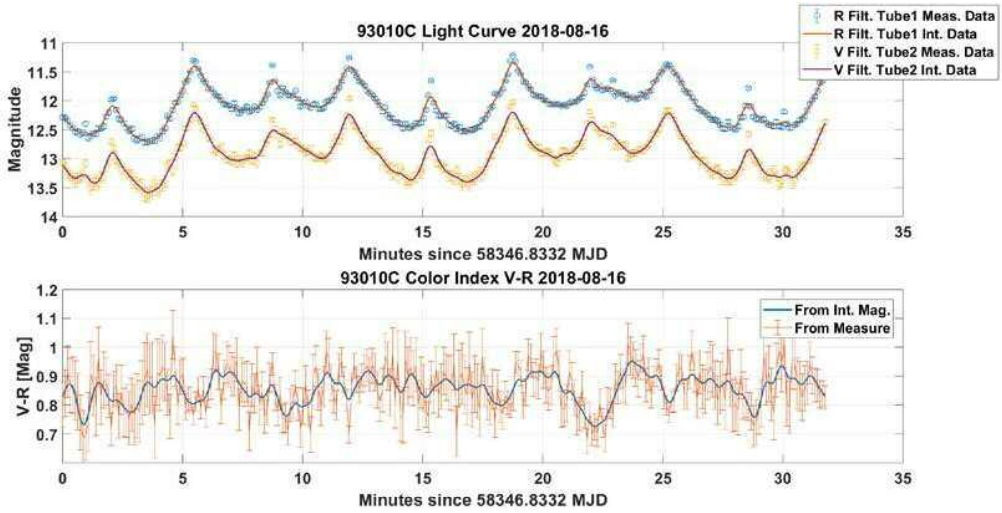

Fig. 11 Light curves with V and R filters extracted for the GLONASS 93010C satellite (top) and color index (bottom).

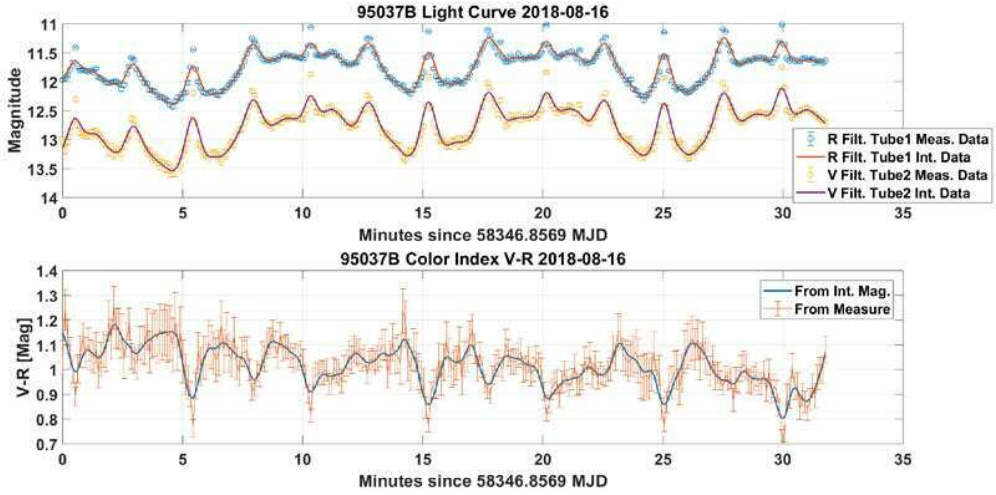

Fig. 12 Light curves with V and R filters extracted for the GLONASS 95037B satellite (top) and color index (bottom).

4.3.2 04053A & 04053B

The last results that we want to show are given in Fig. 13, Fig. 14, and Fig. 15. These belong to the satellites 04053A and 04053B which were launched together, but the first is still an old generation Glonass satellite while the second is a newer version, “Uragan” and “Uragan-M”, respectively [16].

Looking at Fig. 13, one can see how the light curves show similarities with those seen in section 4.3.1, but in this case it is more difficult to identify a rotation period. Nevertheless, it is interesting to see how the trend and the value of the color index in Fig. 13 are comparable with that in Fig. 12, confirming that the color index signature is specific for the physical characteristics and shape of the observed object, information that could be useful for the object identification. The fact that the color index signature is satellite type specific is also confirmed by the comparison of the bottom graph of Fig. 14 with that of Fig. 13. Both satellites have the same age and due to the commonalities of their shape visible in Fig. 3 also their light curves share some similarities. However, the shape and the values of the color indices

are different. Focusing on the first 20 minutes of the color index in Fig. 14 the "sinusoidal" trend previously seen is not present anymore. But a periodical signature, which finds correspondence in the light curve period, could be clearly identified by looking at the behavior from minute 2.5 to 5.5, from 8 to 12, and from 15 to 17.5. This could be due to a different orientation of the spin axis in the body-fixed and/or the inertial frame.

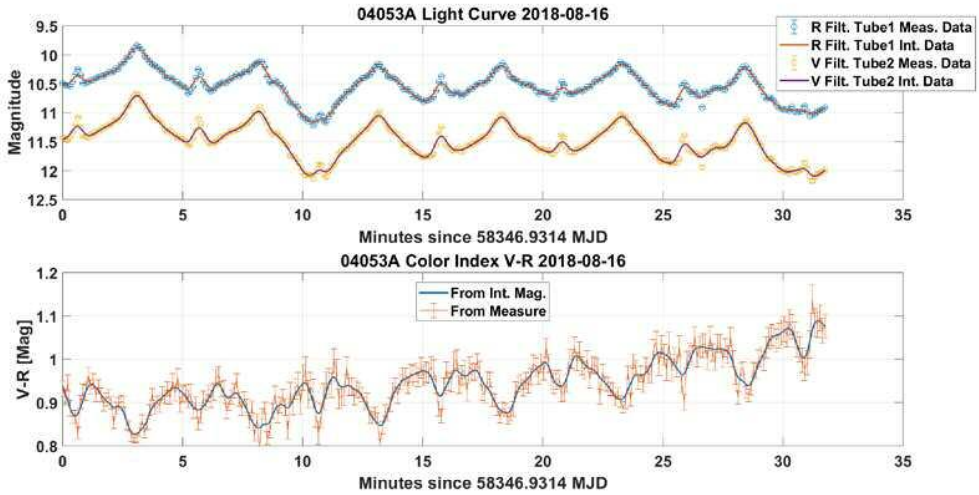

Fig. 13 Light curves with V and R filters extracted for the GLONASS 04053A satellite (top) and color index (bottom).

For completeness, in Fig. 15 we report also the results obtained comparing the B and V light curves for the 04053B case. Looking at the B-V color index we do not see a signal as that visible for the V-R. We notice only a periodical increase of the B-V uncertainty correlated with the faintest points of the B light curve, as expected. However, even if the signal of this color index is hidden within the noise, one can see that this satellite is not reflecting too much in the B wavelength and B-V difference is pretty constant over the time. This information is still useful to understand the surface properties of the object.

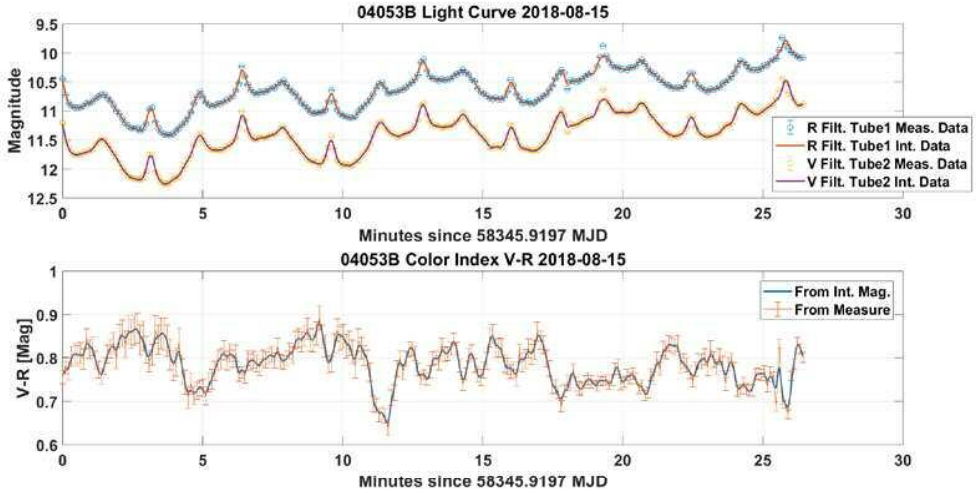

Fig. 14 Light curves with V and R filters extracted for the GLONASS-M 04053B satellite (top) and color index (bottom).

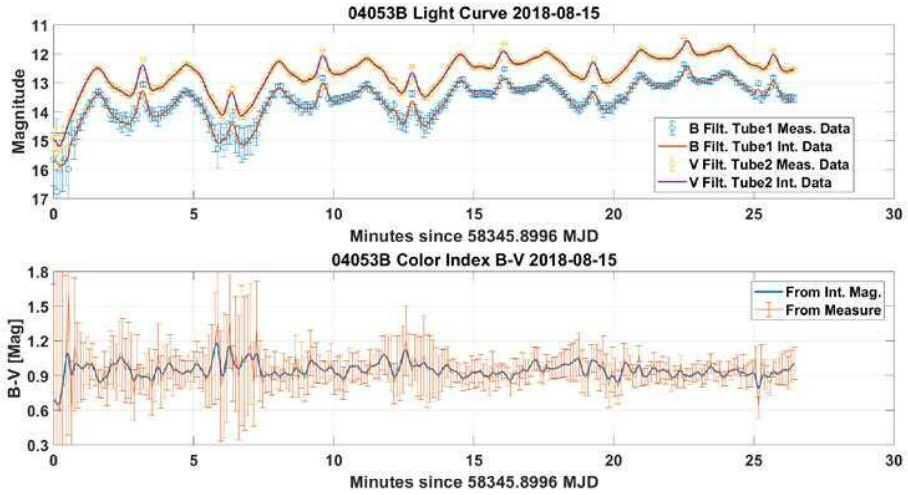

Fig. 15 Light curves with B and V filters extracted for the GLONASS-M 04053B satellite (top) and color index (bottom).

5. CONCLUSIONS AND SENSITIVE POINTS

For future ADR missions for large space debris, such as rocket upper stages and defunct satellites, the knowledge of their attitude state (spin axis orientation in the body-fixed and the inertial frame) is of fundamental importance. A way to retrieve attitude information of space debris from the ground is via the analysis of the variations of reflected light over time. Important information about the attitude can not only be retrieved from the light curves but also from the color of the reflected light. In this study we used the newly installed ZimTWIN telescope at the Zimmerwald observatory to acquire simultaneous light curves in different colors, either B and V, or R and V. The big advantage of this telescope is that the same hardware, in terms of camera and tube, is present twice on the same mount. This guarantees the same performance coming from the two observing systems. We were then able to extract color indices at high temporal resolution from the light curves. This allowed us to evaluate the light reflected in different color bands from the same part of the object under the same illumination conditions, and to discriminate the contribution of the different parts of the satellites to the total amount of reflected light.

The main challenge of this technique is the synchronization of the two cameras. A time shift in the measurement points will cause an increase in the scatter of the color indices. This problem was solved by synchronizing the controllers of the two cameras via the same ntp-server, which allowed us to monitor the time drift between the cameras and correct it via interpolation of the light curves with a smoothing spline. This choice allowed also to obtain smoothed light curves and color indices which facilitate their interpretation.

The S/N is a limiting factor for the color index results and a optimization of the exposure time is required takin care not to undersample the features of interest.

First, we reported the results obtained for 3-axis stabilized active GEO satellites, and then we showed the results obtained for spent upper stages and defunct Glonass satellites. The study of the colors provides information about both attitude and physical characteristics of the observed objects. The color indices show periodical features typical for each type of objects, very often they are also less ambiguous than light curves. This can be employed to validate the estimated rotation period. Their change over time provides information about the contribution of the different portions of the object in the light reflected toward the observer.

Of course, being this a preliminary study, much more can be done: first we have to solve the cameras synchronization problem, which will improve the quality of the color index. Then, one could focus on the merging of the information coming form different color indices, and/or from different telescopes, maybe with different time resolution, which observe the same object synchronously with and without filters. Finally, one could either monitor the same object over time or observe the same type of objects, whose permanence in space is different, to study the aging effect of the space environment, information that could be used to identify a possible parent object of a space debris.

6. REFERENCES

[1] J.-C. Liou and N. Johnson, "Risks in space from orbiting debris," *Science,* vol. 311 (5759), pp. 340-341, January 2006.

[2] K. Wormnes, R. Le Letty, L. Summerer, R. Schonenborg, O. Dubois-Matra, E. Luraschi, A. Cropp, H. Krag and J. Delaval, "ESA technologies for space debris remediation," in *Proceedings of the 6th European Conference on Space Debris*, ESOC, Darmstadt (Germany), 2013.

[3] B. Bastida and H. Krag, "Analyzing the criteria for a stable environment," in *AAS/AIAA Astrodynamics Specialist Conference*, Girwood, Alaska, 2011.

[4] J. Silha, J.-N. Pittet, M. Hamara and T. Schildknecht, "Apparent rotation properties of space debris extracted from photometric measurements," *Advances in Space Research,* vol. 61, no. 3, pp. 844-861, 2018.

[5] J.-N. Pittet, J. Silha and T. Schildknecht, "Spin motion determination of the Envisat satellite through laser ranging measurements from a single pass measured by a single station," *Advances in Space Research,* vol. 61, no. 4, pp. 1121-1131, 2018.

[6] J. Silha, T. Schildknecht, P. J-N., G. Kirchner, M. Steindorfer, D. Kucharski, D. Cerutti-Maori, J. Rosebrock, S. Sommer, L. Leushacke, P. Kärräng, R. Kanzler and H. Krag, "Debris Attitude Motion Measurements and Modelling by Combining Different Observation Techniques," in *Proceedings of the 7th European Conference on Space Debris*, ESOC, Darmstadt (Germany), 2017.

[7] A. Rachman, T. Schildknecht, J. Silha, P. J-N. and A. Vananti, "Attitude State Evolution of Space Debris from Optical Light Curve Observations," in *68th international Astronautical Congress (IAC)*, Adelaide, Australia, 2017.

[8] F. Santoni, E. Cordelli and F. Piergentili, "Determination of Disposed-Upper-Stage Attitude Motion by Ground-Based Optical Observations," *Journal of Spacecraft and Rockets,* vol. 50, no. 3, pp. 701-708, 2013.

[9] L. Bin, Z. Hai-bin and W. Xin, "Photometric Observation and Modeling Study of the Asteroid (26) Proserpina," *Chinese Astronomy and Astrophysics,* vol. 40, no. 3, pp. 373-385, 2016.

[10] H. Cowardin, P. Seitzer, K. Abercromby and E. Barker, "Characterization of Orbital Debris Photometric Properties Derived from Laboratory-Based Measurements," in *Proceedings of the Advanced Maui Optical and Space Surveillance Technologies Conference*, Wailea, Maui, Hawaii., 2010.

[11] A. Rossi, S. Marinoni, T. Cardona, E. Dotto, F. Santoni and F. Piergentili, "The Loiano Campaigns for Photometry and Spectroscopy of Geosynchronous Objects," in *63rd International Astronautical Conference (IAC)*, Naples, Italy, 2012.

[12] P. Seitzer, H. Rodriguez-Cowardin, E. Barker, K. Abercromby, G. Foreman and M. Horstman, "Photometric Studies of GEO Debris," in *Proceedings of the Advanced Maui Optical and Space Surveillance Technologies Conference*, Wailea, Maui, Hawaii, 2009.

[13] T. Cardona, P. seitzer, A. Rossi, F. Piergentili and F. Santoni, "BVRI Photometric Observations and Light-curve Analysis of GEO Objects," *Advances in Space Research,* vol. 58, no. 4, pp. 514-527, 2016.

[14] A. U. Landolt, "UBVRI Photometric Standard Stars Around the Celestial Equator: Updates and Additions," *The Astronomical Journal,* vol. 137, pp. 4186-4269, 2009.

[15] K. Collins, J. Kielkopf, K. Stassun and F. Hessman, "AstroImageJ: Image Processing and Photometric Extraction for Ultra-precise Astronomical Light Curves," *The Astronomical Journal,* vol. 153, no. 2, pp. 77-89, 2017.

[16] G. Krebs, "Gunter's Space Page," [Online]. Available: https://space.skyrocket.de/. [Accessed 25 August 2018].

[17] SpaceFlight 101.com - Space News and Beyond, "Delta IV Medium+ (5,4)," [Online]. Available: http://spaceflight101.com/spacerockets/delta-iv-medium-54/. [Accessed 25 August 2018].

[18] SpaceFlight 101.com - Space News and Beyond, "Atlas V 551," [Online]. Available: http://spaceflight101.com/spacerockets/atlas-v-551/. [Accessed 25 August 2018].

[19] SES, "19.2°E Europe," [Online]. Available: https://www.ses.com/our-coverage/orbital-position/196. [Accessed 25 August 2018].

[20] United Launch Alliance, "United Launch Alliance Marks the 50th Successful GPS Launch for the Air Force with the Delivery of the GPS IIF-2 Mission to Orbit," [Online]. Available:

https://www.ulalaunch.com/missions/2011/07/16/united-launch-alliance-marks-the-50th-successful-gps-launch-for-the-air-force-with-the-delivery-of-the-gps-iif-2-mission-to-orbit. [Accessed 25 August 2018].

[21] United Launch Alliance (ULA), "United Launch Alliance Successfully Launches WGS-7," [Online]. Available: https://www.ulalaunch.com/about/news/2015/07/23/united-launch-alliance-successfully-launches-wgs-7. [Accessed 25 August 2018].